Controlling vortex lattice structure of binary Bose-Einstein condensates via disorder-induced vortex pinning

Dibyendu Kuiri [1,*] Thudiyangal Mithun [2,3] and Bishwajyoti Dey [1]
[1]*Department of Physics, SP Pune University, Pune 411007, India*
[2]*Department of Atomic and Molecular Physics, Manipal Academy of Higher Education, Manipal 576 104, India*
[3]*Department of Mathematics and Statistics, University of Massachusetts, Amherst, Massachusetts 01003-4515, USA*

(Received 18 February 2023; accepted 3 June 2024; published 27 June 2024)

We study the vortex pinning effect on the vortex lattice structure of the rotating two-component Bose-Einstein condensates (BECs) in the presence of impurities or disorder by numerically solving the time-dependent coupled Gross-Pitaevskii equations. We investigate the transition of the vortex lattice structures by changing conditions such as angular frequency, the strength of the inter-component interaction and pinning potential, and the lattice constant of the periodic pinning potential. We show that even a single impurity pinning potential can change the unpinned vortex lattice structure from triangular to square or from triangular to a structure which is the overlap of triangular and square. In the presence of a periodic pinning potential or optical lattice, we observe the structural transition from the unpinned vortex lattice to the pinned vortex lattice structure of the optical lattice. In the presence of a random pinning potential or disorder, the vortex lattice melts following a two-step process by creation of lattice defects, dislocations, and disclinations, with the increase of rotational frequency, similar to that observed for single-component Bose-Einstein condensates. However, for the binary BECs, we show that the two-step vortex lattice melting also occurs with increasing strength of the intercomponent interaction.

DOI: 10.1103/PhysRevA.109.063333

I. INTRODUCTION

Studies of multicomponent Bose-Einstein condensates (BECs), either of the same atomic species [1–5] or of different atomic species [6–9], have become a subject of recent interest. This is because of the fact that the presence of two competing energy scales of intra- and intercomponent interaction, the multicomponent BEC presents novel and fundamentally different ground-state scenarios and vortex lattice structures than that of the single-component BECs. Binary BECs have been realized in various setups: a single isotope in two different hyperfine states [10], two different isotopes of the same alkali metal [7], or two distinct elements [7,11]. By varying the particle numbers of the components, it is possible to go continuously from regimes of interpenetrating superfluids to those with separated phases [12]. The equilibrium vortex lattice structure of rotating single-component BECs is the well-known Abrikosov vortex lattice or triangular (hexagonal) vortex lattice. On the other hand, a rich variety of vortex lattice structures occurs in rotating multicomponent BECs, such as interlaced square vortex lattice which has been observed in rotating spinor BECs [13]. It has been shown that by varying the strength of the intercomponent interaction for binary BECs the interlocked vortex states undergo a phase transition from triangular to square lattices, then to double-core lattices, and finally leading to nonperiodic interwoven serpentine vortex sheets [14–17]. More recently, it has been shown that in rotating binary dipolar BECs a new vortex lattice structure is caused by the long-range interactions [18]. For unequal masses of two species of binary BECs, the two condensates rotate at different speeds due to the disparity in masses and show vortex synchronization leading to the formation of bound pairs and the locked state of the two vortex lattices [19,20]. For attractive interaction between the two components of the binary BECs, the system exhibits nontriangular geometry of the vortex lattices, such as square and two-quantum-vortices [21]. It has been further shown that for unequal masses of the atoms, exotic vortex lattice configurations which include the honeycomb, kagome, and herringbone can exist in binary repulsive BECs [22].

In the past few years, the study of the effect of impurity pinning potential on vortex dynamics in BECs has gained importance. A few examples are vortex lattice melting in the presence of random impurities or disorder and its usefulness to study melting problems, in general [23,24], Anderson localization [25], superfluid behavior [26], turbulent dynamics in BECs induced by stirring mechanism due to time-dependent impurity position [27,28], etc. Rotating BECs with impurities provide a system where it is possible to display, in a controlled way, the interplay between interaction and disorder in the vortex dynamics. This competition is responsible for the vortex lattice melting in BECs, which mimics the observed vortex lattice melting in type II superconductors [29]. Such melting is fundamentally different from the more conventional thermal melting. In this case, the transition can be driven by vortex pinning due to point disorder rather than temperature. It was originally proposed in the context

*Present address: AGH University of Krakow, Academic Centre for Materials and Nanotechnology, al. A. Mickiewicza 30, 30-059 Krakow, Poland.

of vortex matter in high-temperature superconductors [30,31]. High-temperature superconductors have two order parameters, the *s*-wave and *d*-wave order parameters, and the superconductivity of the high-temperature superconductors depends on impurity doping [32]. The vortex dynamics in high-temperature superconductors are described by two-components Ginzburg-Landau theory in the presence of an applied magnetic field [33–36]. The melting process of the vortex lattice in low-temperature superconductors has been studied extensively to explore its role in the critical current of such superconductors. In this context, the study of the impurity-induced vortex pinning and vortex lattice structure in binary BECs is important as it might mimic the vortex lattice dynamics in high-temperature superconductors, which have two order parameters. The identical idea of melting due to random pinning has also been used by Tsiok *et al.* and recently [37] among others. Likewise, the effects of periodic impurities on vortex dynamics in BECs have generated great interest recently due to their applicability in various fields such as the physics of Josephson junction arrays, fractional quantum Hall effect, etc. These studies are done by loading the BECs on a rotating optical lattice, and experiments employing BECs in a rotating optical lattice have led to the observation of some of these physical phenomena [38,39]. For weak optical lattice potential, the pinning of vortices by the optical lattice has shown rich vortex lattice structures [40–44]. Similar studies on honeycomb optical lattices have shown interesting moving vortex phases which are useful for studying the anomalies in the critical current of type II superconductors [45]. Very recently, experimental and theoretical studies of ultracold gases on quasicrystalline optical lattice potential have been reported [46,47]. Quasicrystalline potentials have long-range order but are not periodic. However, very few studies are related to the vortex lattice structures of the binary BECs in the presence of periodic pinning or optical lattice where the presence of the intercomponent interaction further enriches the vortex lattice structures [48,49].

In this paper, we study the effects of impurities or disorder on the equilibrium vortex lattice structures of the rotating binary BECs. The presence of the impurity potential adds another energy scale to the problem besides the other two competing energy scales of intra- and intercomponent interactions in binary BECs. Competition between these energy scales allows controlling the equilibrium vortex lattice structures of the rotating binary BECs via disorder-induced vortex pinning. We show that even a single impurity can change the vortex lattice structure from triangular to square and also from triangular to a distorted lattice. The structure of the pinned vortex lattice depends on the commensurate or incommensurate positions of the impurities w.r.t. the positions of the vortices of the unpinned lattice, i.e., vortex lattice without impurities. Maximum changes in the unpinned vortex lattice structures occur when the impurities are in incommensurate positions. In the presence of periodic impurities or periodic pinning potentials, which can be created by optical lattices, we show that the vortex lattices acquire the structure of the optical lattice due to the pinning of the vortices by the optical lattice potential. In the presence of random impurities or disorder, the vortex lattice melts following a two-step melting process by creating an increasing number of lattice defects, dislocations, and disclinations, with increasing rotational frequency and strength of the random pinning potential. Further, it is shown that the vortex lattice melting of binary BEC in the presence of the disorder is also possible with increasing strength of the intercomponent interaction. To characterize the equilibrium structure of the vortex lattices, we calculate the condensate densities of the components of the binary BEC and its corresponding structure factor profiles. To find the lattice defects in the disordered vortex lattices we plot the Delaunay triangulated disordered vortex lattice showing the lattice defects.

II. THEORETICAL MODEL OF ROTATING BINARY BEC AND THE COUPLED GROSS-PITAEVSKII EQUATIONS FOR THE SYSTEM

We begin with the effective two-dimensional (2D) Gross-Pitaevskii (GP) energy functional $E[\psi_1, \psi_2] = \int \mathcal{E}_{2D}(\mathbf{r})\, d^2r$ expressed in terms of the binary condensate wave functions ψ_j for the jth component ($j = 1, 2$), where the energy density is given by

$$\mathcal{E}_{2D}(\mathbf{r}) = \sum_{j=1}^{2}\left(\frac{\hbar^2}{2m_j}|\nabla\psi_j|^2 + V_j|\psi_j|^2 + \frac{g_{jj}}{2}|\psi_j|^4 - \Omega\psi_j^* L_z\psi_j\right) + g_{12}|\psi_1|^2|\psi_2|^2, \tag{1}$$

where ψ_j^* is the complex conjugate of ψ_j. Here m_j represents the atomic mass of the jth component, $g_{jj} = \frac{4\pi\hbar^2 a_j}{m_j}$ the intracomponent interaction strength, $g_{12} = \frac{2\pi\hbar^2 a_{12}}{m_{12}}$ the intercomponent interaction strength, $m_{12} = \frac{m_1 m_2}{m_1+m_2}$, a_j and a_{12} the corresponding *s*-wave scattering lengths, Ω the rotational frequency, L_z the angular momentum in the z direction, with normalization condition $\int(|\psi_j|^2\, dx\, dy = N_j$, and $N = N_1 + N_2$ the total number of particles in the system. The potential $V_j(x, y)$ consists of two parts $V_j(x, y) = V_{j,\text{trap}}(x, y) + V_{j,\text{impurity}}(x, y)$, the harmonic trap potential and the impurity potential, respectively. The harmonic trap potential has the form $V_{j,\text{trap}}(x, y) = \frac{1}{2}m_j\omega_\perp^2(x^2 + y^2)$, where $\omega_\perp$ is the radial harmonic frequency. For a single impurity at position (x_0, y_0), we take the impurity potential as $V_{j,\text{impurity}}(x, y) = V_{0j}\exp\{\frac{-[(x-x_0)^2+(y-y_0)^2]}{(\sigma/2)^2}\}$, where V_{0j} denotes the strength of the impurity potential interacting with the jth component and σ is the width of the potential. For the periodic distribution of impurities that can be created by the optical lattice, the impurity potential is taken as the optical lattice potential $V_{\text{impurity}} = V_{\text{lattice}}(\mathbf{r}) = \sum_{n_1,n_2} V_0\exp\{\frac{-|\mathbf{r}-\mathbf{r}_{n_1,n_2}|^2}{(\sigma/2)^2}\}$, where $\mathbf{r}_{n_1,n_2} = n_1\mathbf{a}_1 + n_2\mathbf{a}_2$ denotes the lattice points, n_1 and n_2 are integers. For the triangular optical lattice, the two lattice unit vectors are given by $\mathbf{a}_1 = a(0, 1)$ and $\mathbf{a}_2 = a(\pm 1/2, \sqrt{3}/2)$ and for the square optical lattice $\mathbf{a}_1 = a(1, 0)$ and $\mathbf{a}_2 = a(0, 1)$ [42,50]. In the following, we denote the spatial coordinates, time, condensate wave function, rotational frequency, and energies in units of a_h, $\omega_\perp^{-1}$, $a_h^{-3/2}$, $\omega_\perp$, and $\hbar\omega_\perp$, respectively, where $a_h = \sqrt{\hbar/m\omega_\perp}$. From Eq. (1) we obtain the 2D time-dependent

coupled dimensionless GP equations (GPE) as

$$i\frac{\partial}{\partial t}\psi_j(x,y,t) = \Big[-\frac{1}{2}\Big(\frac{\partial^2}{\partial x^2}+\frac{\partial^2}{\partial y^2}\Big)+\tilde{V}_j(x,y) +\tilde{g}_{jj}|\psi_j(x,y,t|^2+\tilde{g}_{12}|\psi_{3-j}(x,y,t)|^2 -\Omega L_z\Big]\psi_j(x,y,t), \quad (2)$$

where $\tilde{g}_{jj}=\frac{4\pi N a_j}{a_h}\sqrt{\frac{\lambda}{2\pi}}$, $\tilde{g}_{12}=\frac{4\pi N a_{12}}{a_h}\sqrt{\frac{\lambda}{2\pi}}$, $\lambda=\frac{\omega_z}{\omega_\perp}$, and $\tilde{V}_j(x,y)=\frac{1}{2}(x^2+y^2)+V_{j,\text{impurity}}(x,y)$. For random impurity potential $V_{1,\text{impurity}}=V_{2,\text{impurity}}=\sum_{n_1,n_2}V_R\exp\{\frac{-[|\mathbf{r}-\mathbf{r}_{n_1,n_2}|^2}{(\sigma/2)^2}\}$, where V_R is drawn from the distribution $[-V_0,V_0)$.

III. NUMERICAL DETAILS

The split-step fast-Fourier method [51] is used to solve the dimensionless coupled GPE equations [Eq. (2)] using imaginary time propagation. We consider the Thomas-Fermi wave function in the absence of rotation, $\psi_{\text{TF}}(x;\Omega=0)$, as the initial condition [52]. Nevertheless, we adjust the wave functions of both components to be slightly different in order to make the initial condition asymmetric. We then introduce the rotation of desired frequency Ω to generate the vortices in the system. In the numerical simulations, we consider 512×512 grid points for a domain size 32×32 and 1024×1024 grid points for a domain size 54×54. We fix both the masses the same and $\tilde{g}_{11}=\tilde{g}_{22}=2000$ unless otherwise mentioned. Additionally, $N_1=N_2$ is considered. Our motivating example is that of a mixture of 2D BECs of ^{87}Rb atoms in the different hyperfine spin states; the mass equality suggests our focus on a scenario of two hyperfine states of the same gas, in particular ^{87}Rb [23]. In the absence of rotation and optical lattice potential, the dimensionless chemical potential can be estimated from the expression $\tilde{\mu}=\sqrt{\frac{\tilde{g}_{11}+\tilde{g}_{12}}{\pi}}$. In full dimension, $\mu=\tilde{\mu}\hbar\omega_\perp$. The parameters varied are the strength of the intercomponent coupling $\delta=\frac{\tilde{g}_{12}}{\tilde{g}_{jj}}$, the rotational frequency Ω, and the strength of the impurity potential. We calculate the structure factors profiles of the vortex lattices in terms of the spatial density of the condensate components as $S_j(\mathbf{k})=\int dx\,dy|\psi_j(x,y,t)|^2e^{i\mathbf{k}\cdot\mathbf{r}}$, $j=1,2$. The structure factor profiles provide information about the periodicity of the condensate density. We also plot the Delaunay triangulated lattice of the condensate densities to determine the number of nearest neighbors of the vortex lattice to show lattice disorder through the creation of the lattice defect dislocations and disclinations. Dislocations are lattice defects consisting of pairs of fivefold or sevenfold and disclinations are isolated fivefold or sevenfold coordinate axes respectively. For finding the dislocations and disclinations the boundary coordinates are not considered. In order to study the effect of random pinning potential due to random impurities or disorder on the vortex lattice, we generate random potential V_{impurity} by considering a square optical lattice $V_{\text{lattice}}(\mathbf{r})$, where we fix the width of each Gaussian peak σ to 0.5 and distance between each peak, a, to 1. The height of each peak, V_0, has been changed with the help of random numbers which are uniformly distributed over $[-V_0,V_0]$ [29].

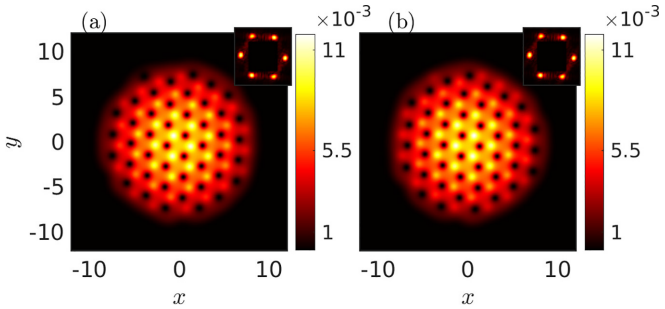

FIG. 1. Condensate densities with color bars (a) $|\psi_1|^2$ and (b) $|\psi_2|^2$ (right) without an impurity for $\delta=0.6$ and $\Omega=0.71$. The corresponding structure factor profiles are given in the inset.

IV. EFFECT OF IMPURITIES OR PINNING CENTERS ON THE EQUILIBRIUM STRUCTURES OF UNPINNED VORTEX LATTICES

A. Effect of single impurity

To see the effect of a single impurity on the vortex lattice structure, we consider the equilibrium vortex lattice in the presence of a single impurity. In the absence of any impurity, the rotating binary BECs with equal intracomponent interaction but varying intercomponent interaction and rotational frequency show rich equilibrium vortex lattice structures [14].

In the presence of an impurity, the vortex lattice structures are expected to get distorted due to the pinning of the lattice vortices with the impurity. We first show that the presence of even a single impurity can change the unpinned equilibrium vortex lattice structures of a binary BEC. We fix the impurity position (x_0,y_0) near the trap center and in the middle of the two vortices of the unpinned triangular vortex lattice as it provides maximum distortion of the vortex lattice. Additionally, we set $V_{01}=V_{02}$.

We choose the interaction parameter between components δ and the rotational frequency Ω, which corresponds to a triangular vortex lattice ([14]). Figure 1 shows the unpinned density profiles of the triangular vortex lattices of the two components. The corresponding structure factor profiles shown in the inset have six peaks as expected for a regular hexagonal Abrikosov lattice.

Interestingly, in the presence of a single impurity, the vortex lattice structures change from triangular to square lattice. This is shown in the density profiles in Fig. 2, and the corresponding structure factor profiles display four peaks as expected for a square lattice structure. This is because the vortices of both components near the impurity compete with each other to become pinned with the impurity. Since the impurity strength $V_0\ll\mu$, neither of the vortices succeeds, and, as a result, the entire vortex lattice rearranges to a square lattice to minimize the lattice potential energy $E_{\text{lattice}}=\langle\psi(x;\Omega)|V_{\text{lattice}}|\psi(x;\Omega)\rangle$.

To understand this transition, we calculated the equilibrium lattice structure starting from a vortex-free ground state and the corresponding lattice potential energies by varying the impurity strength. The results are shown in Fig. 3, where E_{lattice} is normalized with the $E_{\text{lattice0}}=\langle\psi(x;\Omega=0)|V_{\text{lattice}}|\psi(x;\Omega=0)\rangle$. As expected, in the presence of an impurity, the lattice potential energy decreases as a result of the pinning

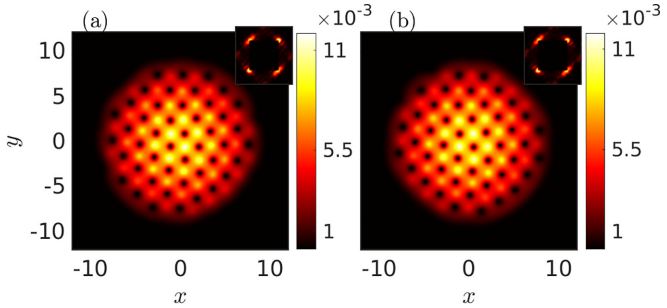

FIG. 2. Condensate densities with color bars (a) $|\psi_1|^2$ and (b) $|\psi_2|^2$ for $\delta = 0.6$, $\Omega = 0.71$ in the presence of a single impurity at $(x_0 = 0, y_0 = -0.5)$ with strength $V_{01} = V_{02} = 1$. The corresponding structure factor profiles are given in the inset.

of the vortex with the impurity. As shown in the figure, there are three regimes with increasing strength of the pinning potential. In the first regime, we get higher E_{lattice}, which remains nearly flat in the second regime. In the third regime, we see a lower E_{lattice} for a further increase in impurity strength. In the first regime, for weaker strength of the impurity potential ($V_0 \ll \mu$) vortices of both components are weakly pinned, resulting in square lattices. In the second regime, V_0 from 3 to 23, we observe the pinning of the vortices of one of the components. However, the square-vortex lattice is unchanged. In the third regime, vortices of both components are pinned at impurity, and as a result, we see maximum vortex lattice distortion.

Figure 4 shows a cross section ($x = 0$ slice) of the density profiles as shown in Fig. 3. The total density $\rho_T = |\psi_1|^2 + |\psi_2|^2$ is also shown in the same figure (black curve). As mentioned above, for weak pinning the vortex lattice undergoes a transition to the square lattice (Fig. 2 and the first figure from the left in the density profiles in Fig. 3) from the unpinned triangular lattice (Fig. 1). A smoother total density ρ_T is favorable for the square lattice [14], which results in the

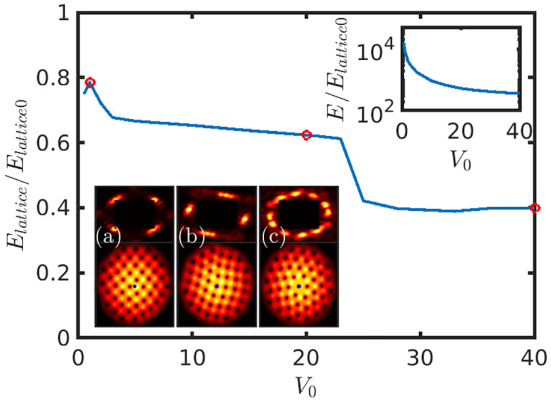

FIG. 3. Lattice energy versus impurity strength for a single impurity placed at $(x_0 = 0, y_0 = -0.5)$. The corresponding vortex lattice and structure factors of one of the components corresponding to the red points are given the bottom left inset (a)–(c), where the blue dot shows the position of a single impurity. The top right inset shows the normalized total energy E/E_{lattice0} calculated from Eq. (1) as a function of the V_0. The other parameters are $\delta = 0.6$ and $\Omega = 0.71$.

shift of the positions of the vortex cores in such a manner that a peak in the density of one component is located in the density hole of the other, resulting in a decrease of $E_{\text{lattice}}/E_{\text{lattice0}}$. This is shown in the cross section plots in Fig. 4(a). With increasing strength of the pinning potential, the vortex lattice becomes more disordered resulting in fluctuations of the total density as shown in Figs. 4(b)–4(f). It is to be noted that the decrease in $E_{\text{lattice}}/E_{\text{lattice0}}$ with well-defined transition points is not quantified in the normalized total energy E/E_{lattice0} as shown in the top right inset of Fig. 3. This further manifests that $E_{\text{lattice}}/E_{\text{lattice0}}$ is the right parameter to quantify a vortex matter transition in presence of a lattice potential [42].

An additional numerical experiment is carried out by considering the ground state of the vortex in Fig. 1 as the initial condition. The final vortex ground state of a V_0 is used as the initial condition for the simulation at $V_0 + \epsilon$, where ϵ denotes a small increment in V_0. This is unlike the case shown in Fig. 3, where the initial condition is always a vortex-free state $\psi_{\text{TF}}(x; \Omega = 0)$. The increase in impurity strength does not affect the geometry of the triangular lattice for $V_0 < 47$, as shown in the inset of Fig. 5. This shows the presence of coexisting solutions for the same parameters set. Moreover, the order-disorder transition of the vortex lattice occurs at a higher strength compared to Fig. 3.

B. Effect of periodic impurities

The vortex lattice structures of the rotating binary BECs can be controlled via the pinning of the vortices by periodic impurities or a periodic pinning potential. Experimentally such effects are created by loading the rotating BECs on a corotating optical lattice [38]. It is well known that the addition of periodic artificial pinning centers helps to realize other vortex arrangements and many dynamical phases [45,53]. In the context of superconductors, vortex pinning due to periodic pinning centers helps in increasing the critical current and controlling the fluxon dynamics [54].

We have simulated the coupled 2D Gross-Pitaevskii equations in the presence of optical lattices of triangular and square geometries. We show that the presence of a weak periodic optical lattice potential leads to a transition from the unpinned vortex lattice structures to the structures of the optical lattice due to the pinning of the vortices by the optical lattice. We show that for binary BECs the intercomponent interaction δ plays a very crucial role in controlling the vortex lattice structures of each component. This is due to the difference in condensate densities produced by the intercomponent interaction.

In cases where the symmetries of the unpinned vortex lattice and the optical lattice are the same, we choose different lattice constants of the two lattices so as to demonstrate the perfect pinning of the unpinned vortex lattice to the optical lattice. After perfect pinning, the lattice constants of the original unpinned lattice match exactly that of the optical lattice.

For example, for the choice of parameters $\delta = 0.2$ and $\Omega = 0.76$, the unpinned vortex lattice is triangular [14] with lattice constants determined by $a = 2.2$, and therefore to show perfect pinning of the vortex lattice, we choose a triangular optical lattice with different lattice constants for $a = 2.28$. Similarly, for $\delta = 0.7$ and $\Omega = 0.76$ the unpinned vortex

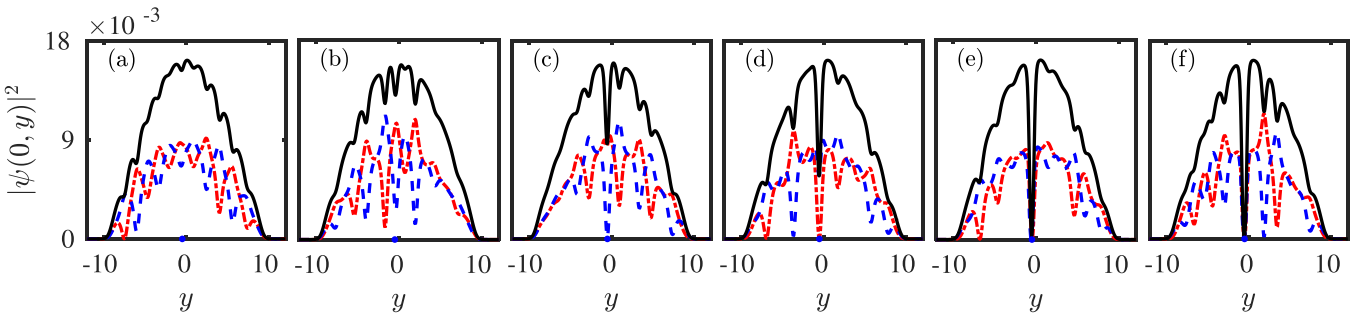

FIG. 4. One-dimensional view of condensate densities $\rho_T(0, y) = |\psi_1|^2 + |\psi_2|^2$ (black), $|\psi_1(0, y)|^2$ (red), and $|\psi_2(0, y)|^2$ (blue) of the cases shown in Fig. 3 for $V_0 = (1, 2, 10, 20, 28, 40)$ (a)–(f).

lattice is square [14] with lattice constants determined by $a = 2.12$, and accordingly to show pinning we choose square optical lattice with different lattice constants $a = 2.20$. We observe that a lower pinning strength of the optical lattice is required for pinning when there is a matching between the symmetries of the unpinned vortex lattice and the optical lattice. To show this we consider pinning of unpinned vortex lattice of various symmetries by a triangular optical lattice with lattice constants determined by $a = 2.28$. For unpinned vortex lattice of different symmetries, we consider cases with increasing values of the intercomponent interaction parameter δ as 0.2, 0.5, and 0.8, keeping the rotational frequency the same as $\Omega = 0.76$. For these cases, the corresponding unpinned vortex lattices are triangular, overlap, and square, respectively [14]. The corresponding triangular pinned vortex lattices are shown in the inset of Fig. 6. From Fig. 6 we can see that increasing the strength of the triangular optical lattice is required for pinning as the symmetry of the unpinned vortex lattice changes from triangular to overlap to square. Figure 6 further shows the respective lattice energies of the unpinned triangular and square lattices for various strengths of the triangular optical lattice. In both cases the lattice energy decreases with the increasing strength of the optical lattice due to pinning. However, for the triangular lattice case, the lowering of the lattice energy is lesser as compared to that of the square lattice case due to the same symmetry of the unpinned vortex lattice and the pinning optical lattice.

Figure 7 shows the pinning of the unpinned square vortex lattice to the square optical lattice with lattice constants determined by $a = 2.12$. For this, we take parameter values as $\delta = 0.7$ and $\Omega = 0.76$ which gives an unpinned square vortex lattice [14] with lattice constants determined by $a = 2.2$. Comparison of Figs. 6 and 7 shows that it requires more strength of the optical lattice to pin a square unpinned vortex lattice to a triangular optical lattice compared to the pinning of a square unpinned vortex lattice to a square optical lattice.

V. EFFECT OF RANDOM IMPURITIES OR DISORDER

In BECs the random impurities or disorder is created and controlled by the laser speckle method [55,56]. For a single-component BEC it has been shown that the vortex lattice melts with increasing strength of disorder due to pinning of the vortices with the random impurities [23]. Also, for a fixed strength of the disorder and with increasing strength of the rotational frequency, the vortex lattice gets increasingly disordered leading to the melting of the vortex lattice. The vortex lattice gets disordered by the creation of lattice defects,

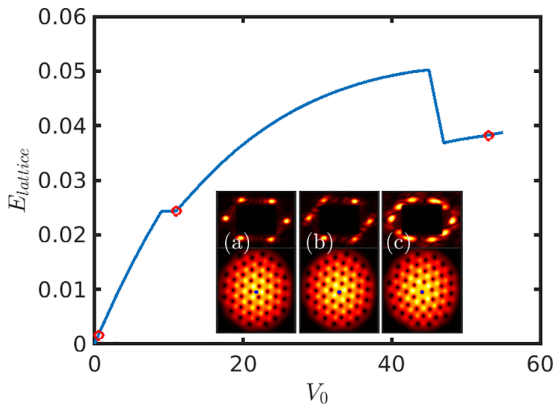

FIG. 5. Lattice energy versus impurity strength for a single impurity placed at $(x_0 = 0, y_0 = -0.5)$ starting from a vortex ground state shown in Fig. 1. The corresponding vortex lattice and structure factors of one of the components corresponding to the red points are given the inset (a)–(c), where the blue dot shows the position of a single impurity.

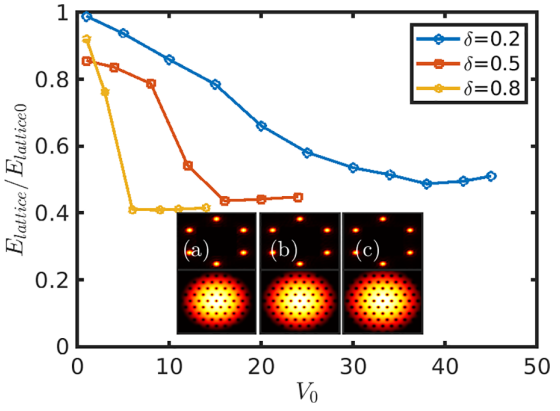

FIG. 6. Lattice energy versus impurity strength for a triangular optical lattice for $\delta = 0.2$, $\delta = 0.5$, and $\delta = 0.8$ for the fixed rotation strength $\Omega = 0.76$ and the lattice constant $a = 2.28$. The condensate density of the first component $|\psi_1|^2$ in the inset shows the pinned triangular vortex lattices for (a) $\delta = 0.2$, $V_0 = 11$, (b) $\delta = 0.5$, $V_0 = 20$, and (c) $\delta = 0.8$, $V_0 = 42$. The second component $|\psi_2|^2$ also exhibits the triangular vortex lattice.

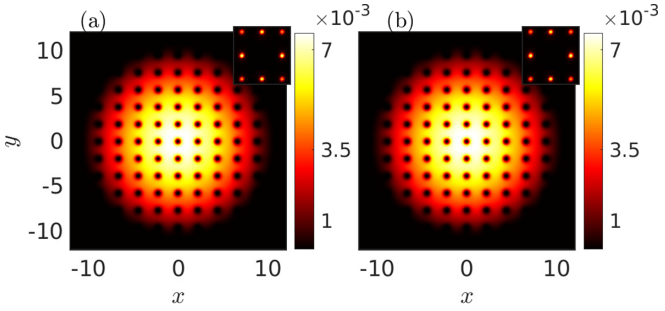

FIG. 7. The condensate densities with color bars (a) $|\psi_1|^2$ and (b) $|\psi_2|^2$ show the pinned square vortex lattices with lattice constant $a = 2.2$ for $\delta = 0.8$, $\Omega = 0.76$ and $V_0 = 35$.

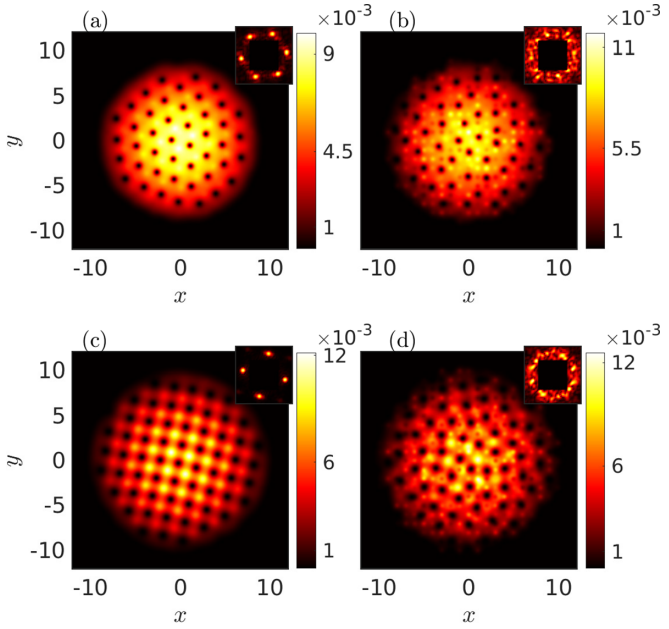

FIG. 8. Condensate density with color bars $|\psi_1|^2$ and structure factor (inset) for (a), (b) $\delta = 0.2$ and (c), (d) $\delta = 0.8$ for the fixed Ω=0.76 with random impurity strength $V_{0j} = 1$ (a), (c), $V_{0j} = 10$ (b), and $V_{0j} = 15$ (d) shows the order to disorder transition of a vortex lattice. The density $|\psi_2|^2$ shows similar pattern.

dislocation, and disclination. Such melting of vortex lattice follows two steps. In the first step, the positional order of the unpinned vortex lattice disappears, but the orientational order is retained. In the second step, both positional and orientational order disappears. In the first step of melting, only dislocations are created whose number increases with increasing rotational frequency, and the second step involves the creation of both dislocations and disclinations [29].

The two-step vortex lattice melting is attributed to the Berezinski-Kosterlitz-Thouless-Halperin-Nelson-Young (BKTHNY) transition [57–60]. The two-step vortex lattice melting has been experimentally observed recently in type II low-temperature superconductors [61,62]. Recent numerical simulations of the dynamics of single-component BECs in the presence of random impurities have also shown two-step vortex lattice melting [29]. For the binary BECs, such studies of disorder-induced vortex lattice melting are important due to their relevance in the context of the investigation of vortex lattice melting in more complex high-temperature superconductors having two order parameters. Besides the possibility of melting the vortex lattice with increasing strength of disorder and rotational frequency similar to that of the single-component BECs, we further show that for the binary BECs, it is also possible to melt the vortex lattices by varying the strength of the intercomponent interaction δ.

To show this we consider random impurities effects on both the triangular as well as the square vortex lattice regimes. Figure 8 shows that for the disorder strength $V_{01} = V_{02} = 1$, the vortex lattices of both components remain nearly hexagonal and square respectively for the cases $\delta = 0.2$ and 0.8 as seen from the density plots and the corresponding structure factor profiles, which show six periodic peaks. But at higher disorder strength, the vortex lattice of both the components gets disordered as seen from the density plots and the structure factor profiles.

Similar to the single-component BECs, the two-step vortex lattice melting by the creation of lattice defects with increasing rotational frequency [29] is also observed for the binary BECs. The corresponding Delaunay triangulated disordered vortex lattice structures are shown in Fig. 9. In the plots, the lattice defects dislocations with fivefold and sevenfold nearest coordinates are shown in black and green-filled circles, respectively, and the disclinations are shown in red-filled circles. From Fig. 9 we can see that for $\Omega = 0.45$ and $\Omega = 0.6$ the lattice defects present for both the components are only the dislocations. In this case, the translational symmetry of the unpinned triangular lattice is lost, but the rotational symmetry is still present. This can be seen from the structure factor profiles in the inset of the figures of the corresponding densities for these two cases. The structure factor profiles for both components show six nearly periodic peaks implying that the rotational invariance of the unpinned triangular lattice is still maintained even in the presence of the random impurities. As the rotational frequency increases further to $\Omega = 0.9$, both types of lattice defects, dislocations, and disclinations are present. The number of lattice defects increases leading to the melting of vortex lattices for both components. With the appearance of disclinations, the rotational invariance is also lost. The structure factor profiles in the inset show that there are more intense peaks corresponding to the disordered vortex lattices.

Similarly, the two-step vortex lattice melting is also observed for different random realizations, and the corresponding plots are not shown here to avoid cluttering the figures.

We have also observed the two-step vortex lattice melting for the binary BECs with increasing strength of the intercomponent interaction δ. This is shown in Fig. 10. From the structure factor profiles in the inset of the figure, we can see that for the intercomponent interaction strengths $\delta = 0.45$ and $\delta = 0.55$ the sixfold rotational symmetry is still preserved. The loss of long-range order with increase in δ can be verified from the orientational correlation function $g_6(r) = (\sum_{i,j} \Theta(\frac{\Delta r}{2} - |r - |\mathbf{r}_i - \mathbf{r}_j||) \cos\{6[\theta(\mathbf{r}_i) - \theta(\mathbf{r}_j)]\}) \times [1/n(r, \Delta r)]$, where $\Theta(r)$ is the Heaviside step function, $\theta(\mathbf{r}_i) - \theta(\mathbf{r}_j)$ is the angle between the bonds located

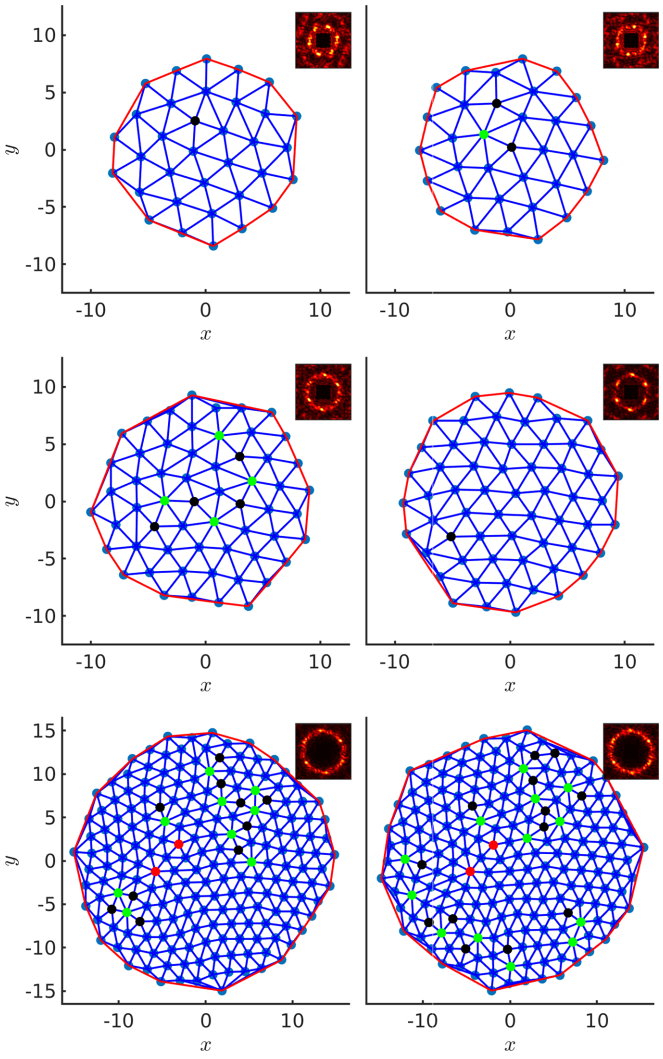

FIG. 9. Top, middle, and bottom panels are Delaunay triangulated disordered vortex lattice of the first (left) and second (right) BEC components for $\delta = 0.2$, $g_{11} = 8000$, and $\Omega = (0.45, 0.6, 0.9)$ respectively and random impurity strength $V_{0j} = 1.5$.

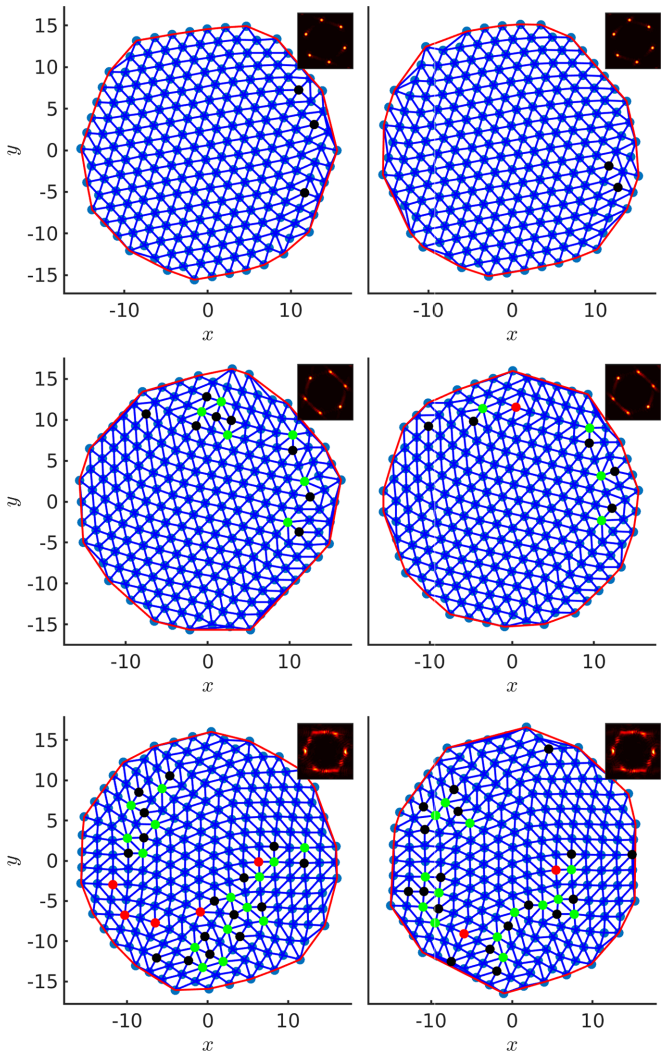

FIG. 10. Top, middle, and bottom panels are Delanuay triangulated disordered vortex lattices of the first (left) and second (right) BEC components for $\Omega = 0.9$, $g_{11} = 8000$, and $V_{0j} = 0.5$ with $\delta = (0.45, 0.55, 0.67)$, respectively.

at $\mathbf{r}_i$ and the bond located at $\mathbf{r}_j$, $n(r, \Delta r) = \sum_{i,j} \Theta(\frac{\Delta r}{2} - |r - |\mathbf{r}_i - \mathbf{r}_j||)$, Δr defines a small window of the size of the pixel around r and the sum is over all the bonds, shown in Fig. 11. The range of variable r is determined by the lateral size of each image. In Fig. 11 we restrict the r to half the lateral size of the image, which corresponds to approximately $7.5a_0$ (where a_0 is the average lattice constant) for $\delta = 0.45$ and $7.6a_0$ for $\delta = 0.55$. The sharp peaks in Fig. 11 correspond to the nearest-neighbor bond distances. Though a power-law decay of the orientational order is expected as a characteristic of a quasi-long-range orientational order [63], the small range of radial distance is not providing any conclusive evidence. The small decay rate of $\delta = 0.45$ as compared to the case of $\delta = 0.55$ indicates the better orientational order of $\delta = 0.45$ case. When the intercomponent interaction strength is increased further to $\delta = 0.67$, both translational and rotational symmetries are lost. The lattice structures of both components become completely disordered, as shown in the corresponding structure factor plots depicted in Fig. 10. We have verified similar results for different random realizations.

VI. SUMMARY, CONCLUSIONS, AND FUTURE CHALLENGES

We have studied how the vortex lattice structures of binary BECs can be controlled by the pinning of the vortices by impurities or disorder. We have considered the pinning effects of three different types of impurities, all of which can be created

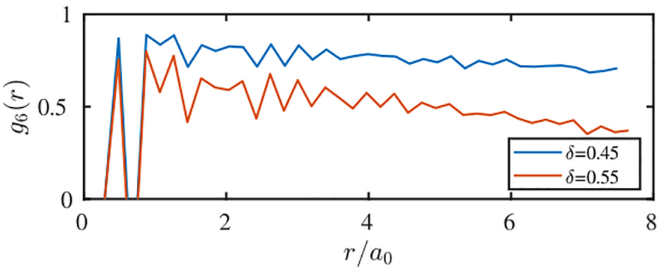

FIG. 11. Orientational correlation function $g_6(r)$ as a function of r/a_0 for $\delta = 0.45$ and $\delta = 0.55$ for a fixed rotation strength corresponds to Fig. 10.

experimentally using laser beams. By numerically solving the time-dependent coupled Gross-Pitaevskii equations we have observed the transition of the ordered unpinned vortex lattice structures to various phases where vortices order in lattice structures of different symmetries, in periodic arrays, as well as in completely disordered or melted lattice. The transitions are determined by the competition between the strengths of the intercomponent interaction, impurity potential, and rotational frequency. The intercomponent interaction plays a very important role in inducing different degrees of disorder in the vortex lattices of the two components due to differences in the densities of the condensate.

In the presence of a single impurity, we observe the transition of the unpinned vortex lattice structure from the triangular to square and to a disordered lattice. For periodic impurities, we have considered the triangular and square optical lattices corotating with the binary BEC. We observed the transition of the unpinned vortex lattices to the pinned lattices where all the vortices are pinned to lattice points. The minimum pinning strength of the optical lattice is required to pin the vortex lattice if there is a matching between the symmetries of the unpinned vortex lattice and the optical lattice. However, it requires a lesser strength of the optical lattice potential to pin a triangular vortex lattice to a triangular optical lattice as compared to the pinning of a square vortex lattice to a square optical lattice. Also, it requires higher strength of the optical lattice potential to pin a triangular vortex lattice to a square optical lattice as compared to the pinning of a square unpinned vortex lattice to a square optical lattice. In the presence of random impurities or disorder, the unpinned vortex lattice melts. The melting and loss of long-range order occur following a two-step melting process by the creation of an increasing number of lattice defects with increasing rotational frequency as well as the strength of the random pinning potential. Interestingly, we observed that similar vortex lattice melting can also occur in binary BECs by increasing the strength of the intercomponent interaction for a much weaker strength of the random pinning potential.

In conclusion, rotating binary BECs in the presence of impurities or disorder provide an interesting system for studying new quantum phases of matter as well as phenomena known from condensed matter in new perspectives. In this context, the results of the impurity-induced vortex lattice structures in binary BECs as reported here are relevant for vortex dynamics in impurity-doped high-temperature superconductors having two order parameters and should be observed when the experimental results on the vortex lattice structures in such complex superconductors are available in the future.

An interesting direction for future work would be a detailed study of the pinned phases of the binary BECs in the presence of recently realized quasicrystalline optical lattices [46]. In comparison to their periodic counterparts, the aperiodic nature of the underlying quasiperiodic potential and the intercomponent interaction are expected to create various intriguing vortex lattice phases. Another possible direction of future research would be to study the dynamical phases of the vortices in periodic pinning potentials that are distinct from the triangular and square potentials. Experiments with periodic pinning arrays such as honeycomb and kagome revealed interesting anomalies in critical currents [64]. Numerical simulation of vortices in honeycomb optical lattices has shown a remarkable variety of dynamical phases that are distinct from triangular and square pinning arrays and can flow in a direction of the driving force due to the depinning of vortices leading to transport [45]. Similar studies for binary BECs will be relevant in the context of experimental observation of anomalous critical current behavior or the peak effect in high-temperature superconductors.

ACKNOWLEDGMENTS

The authors would like to thank Panayotis G. Kevrekidis for fruitful discussions. B.D. would like to thank the Science and Engineering Research Board of India for funding the research, Grant No. CRG/2020/003787.

[1] C. J. Myatt, E. A. Burt, R. W. Ghrist, E. A. Cornell, and C. E. Wieman, Production of two overlapping Bose-Einstein condensates by sympathetic cooling, Phys. Rev. Lett. **78**, 586 (1997).

[2] D. S. Hall, M. R. Matthews, J. R. Ensher, C. E. Wieman, and E. A. Cornell, Dynamics of component separation in a binary mixture of Bose-Einstein condensates, Phys. Rev. Lett. **81**, 1539 (1998).

[3] P. Maddaloni, M. Modugno, C. Fort, F. Minardi, and M. Inguscio, Collective oscillations of two colliding Bose-Einstein condensates, Phys. Rev. Lett. **85**, 2413 (2000).

[4] S. Tojo, Y. Taguchi, Y. Masuyama, T. Hayashi, H. Saito, and T. Hirano, Controlling phase separation of binary Bose-Einstein condensates via mixed-spin-channel Feshbach resonance, Phys. Rev. A **82**, 033609 (2010).

[5] M. Egorov, B. Opanchuk, P. Drummond, B. V. Hall, P. Hannaford, and A. I. Sidorov, Measurement of *s*-wave scattering lengths in a two-component Bose-Einstein condensate, Phys. Rev. A **87**, 053614 (2013).

[6] G. Modugno, M. Modugno, F. Riboli, G. Roati, and M. Inguscio, Two atomic species superfluid, Phys. Rev. Lett. **89**, 190404 (2002).

[7] S. B. Papp, J. M. Pino, and C. E. Wieman, Tunable miscibility in a dual-species Bose-Einstein condensate, Phys. Rev. Lett. **101**, 040402 (2008).

[8] G. Thalhammer, G. Barontini, L. De Sarlo, J. Catani, F. Minardi, and M. Inguscio, Double species Bose-Einstein condensate with tunable interspecies interactions, Phys. Rev. Lett. **100**, 210402 (2008).

[9] D. J. McCarron, H. W. Cho, D. L. Jenkin, M. P. Köppinger, and S. L. Cornish, Dual-species Bose-Einstein condensate of ^{87}Rb and ^{133}Cs, Phys. Rev. A **84**, 011603(R) (2011).

[10] M. R. Matthews, B. P. Anderson, P. C. Haljan, D. S. Hall, C. E. Wieman, and E. A. Cornell, Vortices in a Bose-Einstein condensate, Phys. Rev. Lett. **83**, 2498 (1999).

[11] A. D. Lercher, T. Takekoshi, M. Debatin, B. Schuster, R. Rameshan, F. Ferlaino, R. Grimm, and H. C. Nägerl, Production

of a dual-species Bose-Einstein condensate of Rb and Cs atoms, Eur. Phys. J. D **65**, 3 (2011).
[12] T.-L. Ho and V. B. Shenoy, Binary mixtures of Bose condensates of alkali atoms, Phys. Rev. Lett. **77**, 3276 (1996).
[13] V. Schweikhard, I. Coddington, P. Engels, S. Tung, and E. A. Cornell, Vortex-lattice dynamics in rotating spinor Bose-Einstein condensates, Phys. Rev. Lett. **93**, 210403 (2004).
[14] K. Kasamatsu, M. Tsubota, and M. Ueda, Vortex phase diagram in rotating two-component Bose-Einstein condensates, Phys. Rev. Lett. **91**, 150406 (2003).
[15] K. Kasamatsu, M. Tsubota, and M. Ueda, Vortices in multicomponent Bose-Einstein condensates, Int. J. Mod. Phys. B **19**, 1835 (2005).
[16] K. Kasamatsu and M. Tsubota, Vortex sheet in rotating two-component Bose-Einstein condensates, Phys. Rev. A **79**, 023606 (2009).
[17] K. Kasamatsu and K. Sakashita, Stripes and honeycomb lattice of quantized vortices in rotating two-component Bose-Einstein condensates, Phys. Rev. A **97**, 053622 (2018).
[18] N. Ghazanfari, A. Keleş, and M. O. Oktel, Vortex lattices in dipolar two-component Bose-Einstein condensates, Phys. Rev. A **89**, 025601 (2014).
[19] R. Barnett, G. Refael, M. A. Porter, and H. P. Büchler, Vortex lattice locking in rotating two-component Bose–Einstein condensates, New J. Phys. **10**, 043030 (2008).
[20] R. Barnett, E. Chen, and G. Refael, Vortex synchronization in Bose-Einstein condensates: a time-dependent Gross-Pitaevskii equation approach, New J. Phys. **12**, 043004 (2010).
[21] P. Kuopanportti, J. A. M. Huhtamäki, and M. Möttönen, Exotic vortex lattices in two-species Bose-Einstein condensates, Phys. Rev. A **85**, 043613 (2012).
[22] L. Mingarelli and R. Barnett, Exotic vortex lattices in binary repulsive superfluids, Phys. Rev. Lett. **122**, 045301 (2019).
[23] T. Mithun, K. Porsezian, and B. Dey, Disorder-induced vortex lattice melting in a Bose-Einstein condensate, Phys. Rev. A **93**, 013620 (2016).
[24] I. Guillamón, H. Suderow, A. Fernández-Pacheco, J. Sesé, R. Córdoba, J. M. De Teresa, M. R. Ibarra, and S. Vieira, Direct observation of melting in a two-dimensional superconducting vortex lattice, Nat. Phys. **5**, 651 (2009).
[25] J. Billy, V. Josse, Z. Zuo, A. Bernard, B. Hambrecht, P. Lugan, D. Clément, L. Sanchez-Palencia, P. Bouyer, and A. Aspect, Direct observation of Anderson localization of matter waves in a controlled disorder, Nature (London) **453**, 891 (2008).
[26] M. Könenberg, T. Moser, R. Seiringer, and J. Yngvason, Superfluid behavior of a Bose-Einstein condensate in a random potential, New J. Phys. **17**, 013022 (2015).
[27] T. Mithun, K. Kasamatsu, B. Dey, and P. G. Kevrekidis, Decay of two-dimensional quantum turbulence in binary Bose-Einstein condensates, Phys. Rev. A **103**, 023301 (2021).
[28] T. W. Neely, A. S. Bradley, E. C. Samson, S. J. Rooney, E. M. Wright, K. J. H. Law, R. Carretero-González, P. G. Kevrekidis, M. J. Davis, and B. P. Anderson, Characteristics of two-dimensional quantum turbulence in a compressible superfluid, Phys. Rev. Lett. **111**, 235301 (2013).
[29] T. Mithun, S. C. Ganguli, P. Raychaudhuri, and B. Dey, Signatures of two-step impurity-mediated vortex lattice melting in Bose-Einstein condensates, Europhys. Lett. **123**, 20004 (2018).
[30] J. Kierfeld and V. Vinokur, Erratum: Lindemann criterion and vortex lattice phase transitions in type-II superconductors [Phys. Rev. B 69, 024501 (2004)], Phys. Rev. B **71**, 029901(E) (2005).
[31] V. Vinokur, B. Khaykovich, E. Zeldov, M. Konczykowski, R. A. Doyle, and P. H. Kes, Lindemann criterion and vortex-matter phase transitions in high-temperature superconductors, Physica C: Superconductivity **295**, 209 (1998).
[32] E. Dagotto, Correlated electrons in high-temperature superconductors, Rev. Mod. Phys. **66**, 763 (1994).
[33] M. Karmakar and B. Dey, Reversible magnetization of the layered high-T_c superconductors, Phys. Rev. B **74**, 172508 (2006).
[34] M. Karmakar and B. Dey, Properties of high temperature superconductors in states of mixed symmetry, J. Phys.: Condens. Matter **20**, 255218 (2008).
[35] M. Karmakar and B. Dey, The effect of in-plane mass anisotropy on the properties of high temperature superconductors in states of mixed symmetry, J. Phys.: Condens. Matter **21**, 405702 (2009).
[36] M. Karmakar and B. Dey, Effect of two length scales on the properties of MgB_2 for arbitrary applied magnetic field, J. Phys.: Condens. Matter **22**, 205701 (2010).
[37] E. N. Tsiok, Y. D. Fomin, and V. N. Ryzhov, Random pinning elucidates the nature of melting transition in two-dimensional core-softened potential system, Physica A **490**, 819 (2018).
[38] S. Tung, V. Schweikhard, and E. A. Cornell, Observation of vortex pinning in Bose-Einstein condensates, Phys. Rev. Lett. **97**, 240402 (2006).
[39] R. A. Williams, S. Al-Assam, and C. J. Foot, Observation of vortex nucleation in a rotating two-dimensional lattice of Bose-Einstein condensates, Phys. Rev. Lett. **104**, 050404 (2010).
[40] K. Kasamatsu and M. Tsubota, Dynamical vortex phases in a Bose-Einstein condensate driven by a rotating optical lattice, Phys. Rev. Lett. **97**, 240404 (2006).
[41] H. Pu, L. O. Baksmaty, S. Yi, and N. P. Bigelow, Structural phase transitions of vortex matter in an optical lattice, Phys. Rev. Lett. **94**, 190401 (2005).
[42] T. Sato, T. Ishiyama, and T. Nikuni, Vortex lattice structures of a Bose-Einstein condensate in a rotating triangular lattice potential, Phys. Rev. A **76**, 053628 (2007).
[43] A. Kato, Y. Nakano, K. Kasamatsu, and T. Matsui, Vortex formation of a Bose-Einstein condensate in a rotating deep optical lattice, Phys. Rev. A **84**, 053623 (2011).
[44] O. Morsch and M. Oberthaler, Dynamics of Bose-Einstein condensates in optical lattices, Rev. Mod. Phys. **78**, 179 (2006).
[45] C. Reichhardt and C. J. Olson Reichhardt, Moving vortex phases, dynamical symmetry breaking, and jamming for vortices in honeycomb pinning arrays, Phys. Rev. B **78**, 224511 (2008).
[46] K. Viebahn, M. Sbroscia, E. Carter, J.-C. Yu, and U. Schneider, Matter-wave diffraction from a quasicrystalline optical lattice, Phys. Rev. Lett. **122**, 110404 (2019).
[47] D. Johnstone, P. Öhberg, and C. W. Duncan, Mean-field phases of an ultracold gas in a quasicrystalline potential, Phys. Rev. A **100**, 053609 (2019).
[48] J. W. Reijnders and R. A. Duine, Pinning and collective modes of a vortex lattice in a Bose-Einstein condensate, Phys. Rev. A **71**, 063607 (2005).
[49] M. P. Mink, C. M. Smith, and R. A. Duine, Vortex-lattice pinning in two-component Bose-Einstein condensates, Phys. Rev. A **79**, 013605 (2009).

[50] T. Mithun, K. Porsezian, and B. Dey, Pinning of hidden vortices in Bose-Einstein condensates, Phys. Rev. A **89**, 053625 (2014).
[51] T. Mithun and K. Kasamatsu, Modulation instability associated nonlinear dynamics of spin–orbit coupled Bose–Einstein condensates, J. Phys. B: At. Mol. Opt. Phys. **52**, 045301 (2019).
[52] C. J. Pethick and H. Smith, *Bose–Einstein Condensation in Dilute Gases* (Cambridge University Press, Cambridge, 2008).
[53] M. F. Laguna, C. A. Balseiro, D. Domínguez, and F. Nori, Vortex structure and dynamics in kagomé and triangular pinning potentials, Phys. Rev. B **64**, 104505 (2001).
[54] B. Aichner, B. Müller, M. Karrer, V. R. Misko, F. Limberger, K. L. Mletschnig, M. Dosmailov, J. D. Pedarnig, F. Nori, R. Kleiner *et al.*, Ultradense tailored vortex pinning arrays in superconducting $YBa_2Cu_3O_{7-\delta}$ thin films created by focused he ion beam irradiation for fluxonics applications, ACS Appl. Nano Mater. **2**, 5108 (2019).
[55] L. Sanchez-Palencia and M. Lewenstein, Disordered quantum gases under control, Nat. Phys. **6**, 87 (2010).
[56] A. Ghosal, M. Randeria, and N. Trivedi, Inhomogeneous pairing in highly disordered *s*-wave superconductors, Phys. Rev. B **65**, 014501 (2001).
[57] J. M. Kosterlitz and D. J. Thouless, Ordering, metastability and phase transitions in two-dimensional systems, J. Phys. C **6**, 1181 (1973).
[58] B. I. Halperin and D. R. Nelson, Theory of two-dimensional melting, Phys. Rev. Lett. **41**, 121 (1978).
[59] D. R. Nelson and B. I. Halperin, Dislocation-mediated melting in two dimensions, Phys. Rev. B **19**, 2457 (1979).
[60] L. Pauchard, D. Bonn, and J. Meunier, Dislocation-mediated melting of a two-dimensional crystal, Nature (London) **384**, 145 (1996).
[61] S. C. Ganguli, H. Singh, I. Roy, V. Bagwe, D. Bala, A. Thamizhavel, and P. Raychaudhuri, Disorder-induced two-step melting of vortex matter in co-intercalated $NbSe_2$ single crystals, Phys. Rev. B **93**, 144503 (2016).
[62] I. Roy, S. Dutta, A. N. Roy Choudhury, S. Basistha, I. Maccari, S. Mandal, J. Jesudasan, V. Bagwe, C. Castellani, L. Benfatto, and P. Raychaudhuri, Melting of the vortex lattice through intermediate hexatic fluid in an $a-$MoGe thin film, Phys. Rev. Lett. **122**, 047001 (2019).
[63] S. Chandra Ganguli, H. Singh, G. Saraswat, R. Ganguly, V. Bagwe, P. Shirage, A. Thamizhavel, and P. Raychaudhuri, Disordering of the vortex lattice through successive destruction of positional and orientational order in a weakly pinned $Co_{0.0075}NbSe_2$ single crystal, Sci. Rep. **5**, 10613 (2015).
[64] D. J. Morgan and J. B. Ketterson, Asymmetric flux pinning in a regular array of magnetic dipoles, Phys. Rev. Lett. **80**, 3614 (1998).